Resource

Chemistry & Biology

Molecular Tattoo: Subcellular Confinement of Drug Effects

Graphical Abstract

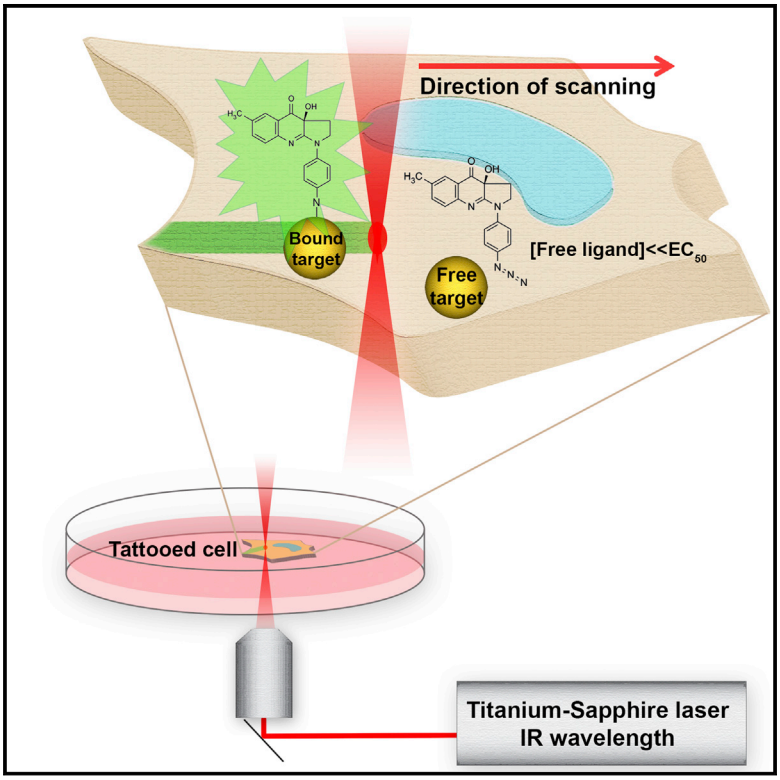

Authors

Miklós Képiró, Boglárka H. Várkuti, ..., Máté Varga, András Málnási-Csizmadia

Correspondence

malnalab@yahoo.com

In Brief

Képiró et al. present an optopharmacological tool, molecular tattooing, which enables in vivo subcellular localization of drug effects. They apply two-photon microscopy for covalent enrichment of photoreactive drugs on specific targets, confining drug effects solely to the irradiated area.

Highlights

- Target-specific drug effect confinement by photoaffinity labeling with 2P-microscopy
- Subfemtoliter precision of permanent effect localization in vivo
- No systemic and side effects outside the targeted area
- Cellular and subcellular targeting of non-muscle myosin 2 in zebrafish and M2 cells

Képiró et al., 2015, Chemistry & Biology 22, 548–558
April 23, 2015
http://dx.doi.org/10.1016/j.chembiol.2015.03.013

CellPress

CellPress

Chemistry & Biology
Resource

Molecular Tattoo: Subcellular Confinement of Drug Effects

Miklós Képiró,[1,6] Boglárka H. Várkuti,[1,6] Anna A. Rauscher,[1,5] Miklós S.Z. Kellermayer,[2] Máté Varga,[3] and András Málnási-Csizmadia[1,4,5,*]

[1]Department of Biochemistry, Eötvös Loránd University, 1117 Budapest, Hungary
[2]Department of Biophysics and Radiation Biology, MTA-SE Molecular Biophysics Research Group, Semmelweis University, 1094 Budapest, Hungary
[3]Department of Genetics, Eötvös Loránd University, 1117 Budapest, Hungary
[4]MTA-ELTE Molecular Biophysics Research Group, Department of Biochemistry, Eötvös Loránd University, 1117 Budapest, Hungary
[5]Optopharma Ltd., 1015 Budapest, Hungary
[6]Co-first author
*Correspondence: malnalab@yahoo.com
http://dx.doi.org/10.1016/j.chembiol.2015.03.013

SUMMARY

Technological resources for sustained local control of molecular effects within organs, cells, or subcellular regions are currently unavailable, even though such technologies would be pivotal for unveiling the molecular actions underlying collective mechanisms of neuronal networks, signaling systems, complex machineries, and organism development. We present a novel optopharmacological technology named molecular tattooing, which combines photoaffinity labeling with two-photon microscopy. Molecular tattooing covalently attaches a photoreactive bioactive compound to its target by two-photon irradiation without any systemic effects outside the targeted area, thereby achieving subfemtoliter, long-term confinement of target-specific effects in vivo. As we demonstrated in melanoma cells and zebrafish embryos, molecular tattooing is suitable for dissecting collective activities by the separation of autonomous and non-autonomous molecular processes in vivo ranging from subcellular to organism level. Since a series of drugs are available for molecular tattoo, the technology can be implemented by a wide range of fields in the life sciences.

INTRODUCTION

The simultaneous temporal and spatial confinement of drug effects within a well-defined area of a living organism has been a long-standing aim in biology. The precise timing of compound release by uncaging was one of the first milestones toward this aim. The uncaging technique proved to be extremely successful for observing fast biological processes by their rapid manipulation in time (Kaplan and Somlyo, 1989; McCray et al., 1980; McCray and Trentham, 1989) and it is still a useful and popular in vitro method for rapid enzyme kinetic studies (Artamonov et al., 2013). The method enables us to manipulate the active concentrations of small molecules, peptides, or nucleic acids (Mayer and Heckel, 2006; Nguyen et al., 2006), track dynamic processes in vivo, or enhance imaging by applying photo-caged fluorescent compounds (Guo et al., 2008). In the process of uncaging, a protecting group is photolyzed by a UV flash and the bioactive compound is released. To enable better spatial resolution, the UV flash lamps and lasers used for uncaging were combined with confocal microscopy (Augustine, 1994; Parker and Ivorra, 1993). However, the in vivo application of uncaging is seriously limited by the systemic effects and side effects of the application of high concentrations of the caged compounds ($\gg EC_{50}$), the limited penetration depth of UV light into different tissues, and the accompanying high phototoxicity along the entire optical axis (Denk et al., 1994). In the 90s, two-photon microscopy (2PM) was invented and soon it also became a suitable tool for the photolysis of caged compounds with several advantages over confocal microscopy: (1) infrared wavelengths (700–1000 nm with Ti:Sa lasers) are less phototoxic, (2) they penetrate deeper into tissues, (3) even subfemtoliter spatial resolution of the photoreaction can be achieved, and (4) the small focal volume further decreases photodamage to the samples (Denk et al., 1994, 1990; Williams et al., 1994). However, the systemic and side effects due to the high concentration of caged compound remained a serious limitation of the uncaging technique (Maier et al., 2005; Matsuzaki et al., 2010). Furthermore, uncaging triggers a localized, but very short, transient effect of the bioactive compound due to the millisecond timescale diffusion of the uncaged compounds from the targeted area. Therefore, in vivo uncaging has become a useful but restricted approach in optopharmacology (Kramer et al., 2013), applied mainly in neuroscience, where such short perturbations of the concentration of bioactive compounds are physiologically relevant.

While uncaging introduces the ligand to the active site of the protein only temporarily, photoaffinity labeling (PAL), developed in the late 1960s, permanently attaches ligands to their targets (Fleet et al., 1969; Singh et al., 1962). In PAL, photoreactive derivatives of bioactive compounds are covalently photo-cross-linked to their targets by UV light. The permanent complex formation by PAL combined with radioactive or fluorescent labeling has been widely implemented to identify targets and characterize binding sites of bioactive compounds both in vitro and in vivo (Geurink et al., 2012; Vodovozova, 2007). Since saturation

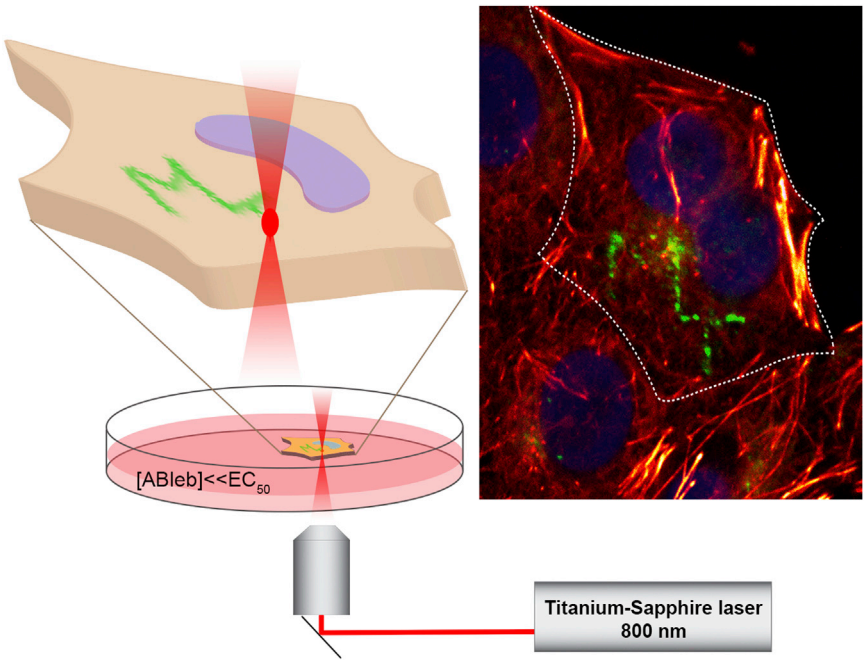

Figure 1. Molecular Tattoo: Spatiotemporal Targeting in Live Cells

The letters MT were engraved into a live single HeLa cell in the presence of 1 μM ABleb (<EC_{50}) by 2PM (λ_{ex} = 800 nm) (schematic representation of the process in the left panel). 2PM image of the subcellular molecular tattoo generated is presented in the right panel. The tattooed ABleb-myosin 2 covalent complex is fluorescent (green), while the actin network is labeled with Actin Glow dye (orange). Nuclei were visualized by Hoechst staining (blue).

of the target requires relatively high concentrations (>EC_{50}) of the photoreactive compound, the application of ligands with low solubility was limited in PAL. To overcome this limitation, sequential PAL (sequential covalent crosslinking) has been introduced recently, whereby multiple photo-crosslinking cycles at low concentrations of the photoreactive ligand enable covalent saturation of target enzymes (Kepiro et al., 2012). We have realized that the combination of sequential PAL with the instrumentation of 2PM-based uncaging offers an unprecedented opportunity for in vivo spatiotemporal confinement of drug effects. A prerequisite for this combination is to confirm that UV-induced PAL crosslinking reactions can also be initiated by 2P excitation. Recently, 3D fluorescence images were generated by 2P irradiation in polyethylene glycol and gelatin matrices containing aryl-azide compounds, however, no direct evidence was presented for the 2P-induced photo-crosslinking reaction (Li et al., 2013; Stoianov and Robinson, 2012). In the current study, we provide direct evidence of a 2P-initiated photo-crosslinking reaction. Moreover, we also show that specific crosslinking can be formed between a photoreactive azidated ligand and its target enzyme by 2P photoinduction.

On the basis of these findings, we introduce molecular tattooing, a new in vivo field of optopharmacology, which enables subfemtoliter, long-term confinement of drug effects by the covalent attachment of azidated ligands to their targets by 2P irradiation (Figure 1). The deep penetration and non-toxic property of 2P irradiation will allow researchers to modulate specific ligand effects in time and space in a wide variety of animal models. Molecular tattooing is not accompanied by side effects or systemic effects of the drug outside the targeted area, because, like sequential PAL, it applies low concentrations of the photoreactive ligand (≪EC_{50}). At these low concentrations, multiple 2P laser scanning of the targeted area results in covalent saturation of the target enzyme by its ligand only within the optically exposed confinement. The process provides permanent, irreversible inhibition or activation of the target exclusively in the irradiated area.

In this study, we characterize the 2P-initiated crosslinking reactions and the resolution of the spatial control of the reaction in the 2PM. The in vivo crosslinking reaction is optimized by varying the concentrations of the applied ligand and the laser scanning parameters. We demonstrate the potential of molecular tattooing by in vivo targeting of myosin 2 in the developing lateral line organ of zebrafish embryos with a photoreactive myosin 2-specific inhibitor, azido-blebbistatin (ABleb). In addition, the precise spatial confinement of myosin 2 inhibition by molecular tattooing is also demonstrated by subcellular targeting of myosin 2 in blebbing human melanoma cells (M2). These experiments illustrate that molecular tattooing is an empowering, novel, in vivo technique for investigating the role of single cells in collective cellular processes and for unveiling local, specific molecular processes within the cell at subfemtoliter resolution.

RESULTS

Characterization of the 2P-Induced Photoreaction of Azidated Compounds

We tested the efficiency of 2P photoactivation of aromatic azidated compounds on azidofluorescein (AFluo) (Salic and Mitchison, 2008) and the photoreactive myosin 2 inhibitor, ABleb (Kepiro et al., 2012). The molecules were dissolved in DMSO, loaded into glass capillaries, and irradiated in the 2PM at 800 nm. The efficiency of the photoreaction at different laser powers was quantified by liquid chromatography-mass spectrometry (LC-MS) (Figure 2A). We found that photoactivations of the compounds were proportional to the square of the focused laser power, indicating the 2P effect (Zipfel et al., 2003). Moreover, defocusing the laser beam completely abolished photoactivation, which further confirmed the 2P-induced photoreaction by the focused laser beam. Since ABleb is a push-and-pull fluorophore (i.e. the quenched fluorescence of blebbistatin due to azido substitution is restored by photo-crosslinking), its fluorescence increases 8.5-fold upon covalent binding to proteins (Figures 2B and 2C). This feature of ABleb and other azidated push-and-pull fluorophores provides a unique tool to determine

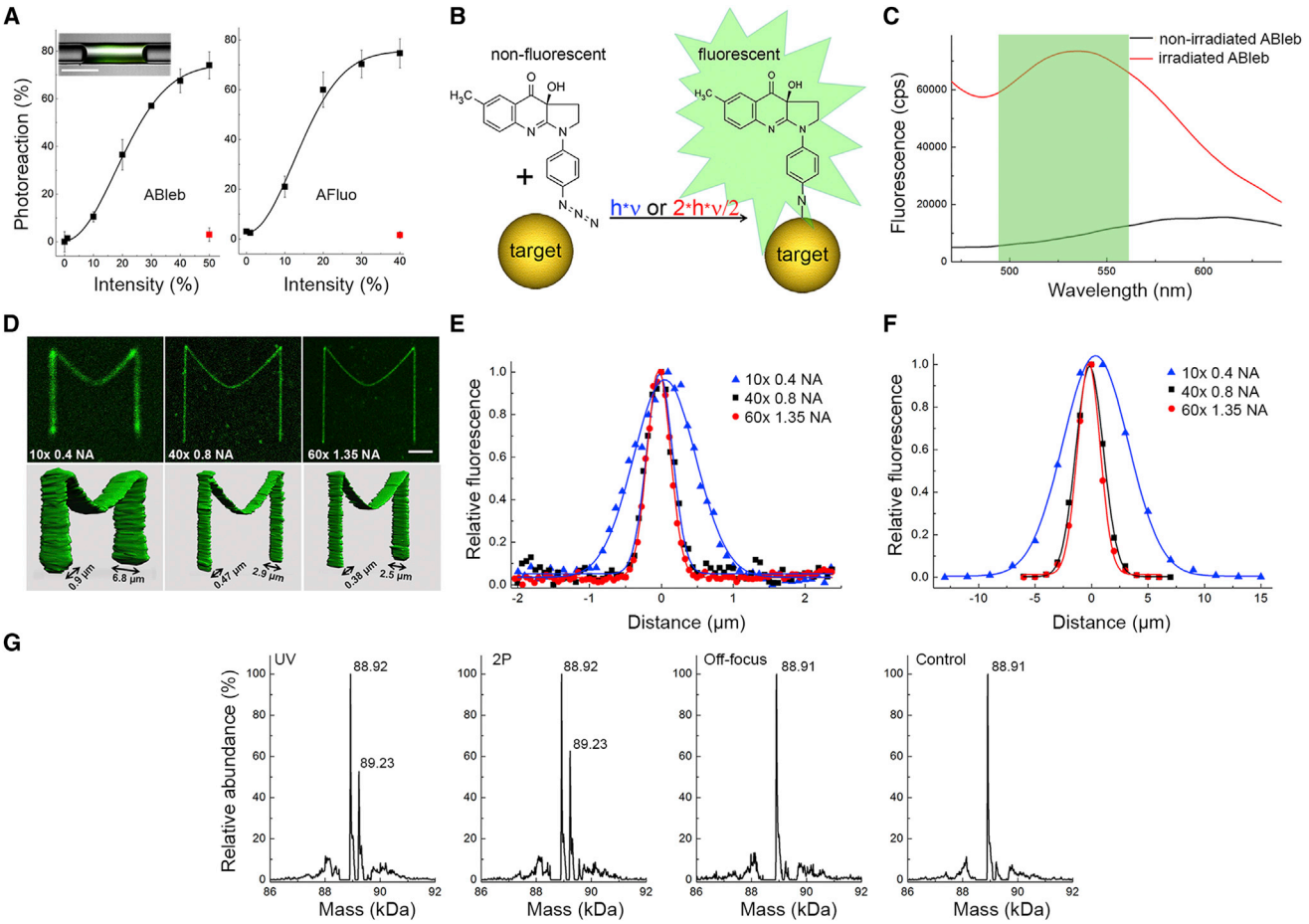

Figure 2. 2P-Induced Photoreaction of ABleb and AFluo and Non-specific and Specific Photo-crosslinking of ABleb

(A) Photoreaction efficiency of ABleb and AFluo determined by LC-MS following 800 nm 2P irradiation as a function of laser power using either focused (black squares) or off-focused (control, red square) laser beams. Inset: ABleb solution in a glass capillary used for 2P irradiation. Data are means ± SD (n = 3). Scale bar represents 500 µm.

(B) A schematic diagram of fluorescence enhancement represented by the transparent green area upon 2P-initiated covalent target-binding of ABleb.

(C) Fluorescence emission spectra of ABleb prior to and following irradiation. The green area indicates the detection range of the green channel of the 2PM.

(D) Confined photo-crosslinking of ABleb to gelatin by line scanning with 2PM. Projections of maximum fluorescence intensity^2 of z-stack images (upper panels) and 3D-rendered surface representations of the V_{2PR} (lower panels) were recorded with three different objective lenses. Double arrows indicate the focal plane (xy) and z axis dimensions of the V_{2PR} (FWHM values of the Gaussian fits to the fluorescence intensity^2 profiles) (Zipfel et al., 2003). Scale bar represents 5 µm.

(E and F) Gaussian fits to the x axis (E) and z axis (F) fluorescence intensity^2 profiles of the z-stack images in (D).

(G) MS spectra of myosin 2 motor domain without irradiation (Control) or irradiated in the presence of ABleb at 300 nm (UV), 800 nm (2P), and 800 nm by off-focus 2PM (Off-focus). 88.91 and 88.92 kDa correspond to non-irradiated and irradiated myosin 2 motor domains, respectively, while 89.23 kDa is the mass of the ABleb-crosslinked myosin (88.92 + 0.305 kDa). Accuracy of MS measurement is ±5 Da.

the effective two-photon reaction volume (V_{2PR}) of the 2PM. Using the line-scan function of the 2PM, "M" letter shapes were tattooed at 800 nm into gelatin matrices containing ABleb, using different objectives to compare their resolutions in the molecular tattoos (Figure 2D). After irradiation, the targeted areas were imaged by z sectioning and the x, y, and z dimensions of the V_{2PR} were determined from the fluorescence intensity^2 profiles of the tattooed lines (Figures 2E and 2F). Laser power for imaging was one magnitude lower compared with the tattooing laser intensity, therefore significant photoreaction did not occur during image laser scanning. In the case of the 1.35 NA objective, we achieved 0.38 µm and 2.5 µm full-width at half maximum (FWHM) resolutions in the xy, and z dimensions, respectively, representing 0.21 fl tattooed volume (V_{2PR}) (Table 1).

To confirm and prove directly that a PAL crosslinking reaction can be induced by 2PM, purified myosin 2 motor domain was illuminated with UV light and 2P in the presence of ABleb. By using LC-MS, we detected covalent bond formation between myosin (88.92 kDa) and ABleb (305 Da) both by UV and 2P irradiation (89.23 kDa on Figure 2G). The control experiment further confirmed the 2P effect, i.e. the off-focus 2P irradiation of the ABleb-treated myosin sample did not induce PAL, because even though the total number of photons reaching the sample was obviously not affected, photon density did not reach the critical value required for 2P reactions. The 10-Da difference in the MS spectra between the control and the irradiated uncrosslinked myosin population is possibly due to a non-specific photo-induced modification of the myosin molecule.

Table 1. Physical Parameters of the Effective Two-Photon Reaction Volumes (V_{2PR})

Objective	ω_{xy} (μm)	ω_z (μm)	$FWHM_{xy\ axis}$ (μm)	$FWHM_{z\ axis}$ (μm)	V_{2PR} (μm^3)
10×/1.35 NA	0.67	4.56	0.92	6.81	11.4
40×/0.8 NA	0.25	1.51	0.47	2.87	0.52
60×/0.4 NA	0.18	1.14	0.38	2.47	0.21

Gaussian fits to the focal plane (xy) and z axis fluorescence intensity^2 profiles of the z-stack images (Figures 2E and 2F) yielded the lateral (ω_{xy}) and axial (ω_z) 1/e radii and FWHM values. V_{2PR} was calculated on the basis of $V_{2PR} = \pi^{3/2}\omega^2_{xy}\,\omega_z$ (Equation 2 from Zipfel et al., 2003).

Molecular Tattooing In Vivo: Spatiotemporal Inhibition of Myosin 2 in the Developing Lateral Line Organ of Zebrafish Embryos

The potential of molecular tattooing in live animal experiments was tested on the migrating posterior lateral line primordia (pLLp) of live zebrafish embryos, which deposit neuromasts at regular intervals along two sides of the body (Figure 3A). Its relative simplicity, well-defined migratory behavior, and good accessibility make the zebrafish pLLp a prime model for studying intra-organ patterning and collective cell migration (Friedl and Gilmour, 2009; Ma and Raible, 2009). Recent studies showed that inhibition of non-muscle myosin 2 by systemic blebbistatin treatment causes aberrant lateral line formation (Ernst et al., 2012). Our aim was to test whether local myosin 2 inhibition of the pLLp affects organ development.

In molecular tattooing in vivo, the threshold concentration at which the pharmacological effects of the photoreactive drug are not yet exerted in the dark (<EC_{50}) has to be determined. Accordingly, in order to determine the dose-response curve, we treated *cldnb:gfp* (Haas and Gilmour, 2006) zebrafish embryos with increasing concentrations of ABleb in the dark and the migration of the pLLp from behind the ear to the tip of the tail was followed (Figure 3B). In the systemic treatment above the EC_{50}, further phenotypic effects were detected, i.e. heart edema, curved body shape, decreased migration of melanocytes, which may also be related to myosin 2 inhibition, since their dependence on ABleb concentration was similar to that of pLLp migration inhibition. The relative migration distances of the pLLps were determined by comparison with the distance between the ear and the tip of the tail and plotted as a function of increasing ABleb concentration (Figure 3C). The fitted dose-response curve to data for ABleb-treated embryos yielded an EC_{50} value of 3.8 ± 0.9 μM, which is similar to that of animals treated with non-photoreactive para-nitroblebbistatin (NBleb) (Képiró et al., 2014) (2.6 ± 0.2 μM). NBleb, which has a highly similar chemical character to ABleb but is not photoreactive, was used as a control for ABleb. Importantly, NBleb has identical inhibitory properties and biological effects as ABleb or blebbistatin, but lacks the photo- and cytotoxic effects of blebbistatin (Képiró et al., 2014; Kolega, 2004). On the basis of the dependence of ABleb concentration on pLLp migration, we applied 1 μM ABleb for tattooing of the pLLp. The fluorescence increase resulting from ABleb-myosin 2 covalent complex formation could be detected even next to the GFP signal of the pLLp. During 2P irradiation, rapid GFP photobleaching was followed by a fluorescence increase due to the photoreaction of ABleb. In the control, only GFP photobleaching was detected upon 2P irradiation in the presence of the non-photoreactive NBleb (Figure 3D). In order to see the phenotypic effect of local inhibition of myosin 2 in the pLLp, we tattooed ABleb into one of the pLLps of a 36-hpf (hours post fertilization) embryo and followed lateral line formation for 12 hr (Figure 3E; Movie S1). In the control experiment, in the presence of 1 μM non-photoreactive NBleb, the pLLp was 2P irradiated under the same conditions as in the tattooing experiment and no effect was observed compared with the lateral line development of the untreated zebrafish. The ABleb-tattooed pLLp moved more slowly and stopped earlier than the non-tattooed pLLp located on the other side of the fish. Furthermore, we found that the number of neuromasts deposited was not affected by local myosin 2 inhibition, therefore distances between the neuromasts were shorter compared with the non-inhibited pLLp. Interestingly, the neuromast pairs on the tattooed and non-tattooed sides were deposited at approximately the same time, suggesting that the temporal synchronization of neuromast formation is independent of myosin 2. Importantly, systemic treatment with a high concentration of the non-photoreactive NBleb (10 μM) resulted in a phenotype similar to that of the tattooed pLLp (Figure 3E). These results indicate that myosin 2 has an autonomous role in lateral line development, since myosin 2 activity is needed solely in the migrating pLLp. In addition, neuromast formation and deposition could be decoupled by local myosin 2 inhibition leading to a further, more general conclusion that these processes are independent from the spatial cues around pLLp, because the number and the morphology of deposited neuromasts were independent of their location in the embryo. Molecular tattooing of the developing lateral line organ clearly demonstrates that this technology enables us to decouple specific, local processes of a complex organ formation and distinguish autonomous and non-autonomous activities of a specific enzyme; this could not be achieved by other methods.

Cellular and Subcellular Tattooing of Blebbing Human Melanoma Cells

To explore the potential of molecular tattooing within single cells and subcellular regions, we studied the function of non-muscle myosin 2 in the mechanism of blebbing of the human melanoma M2 cell line (Salic and Mitchison, 2008; Stoianov and Robinson, 2012). The activity of non-muscle myosin 2 is essential for blebbing (Charras et al., 2005; Cheung et al., 2002; Straight et al., 2003), which is a common feature during apoptosis, cytokinesis, or cell spreading (Charras and Paluch, 2008; Fackler and Grosse, 2008).

In the course of molecular tattooing, M2 cells were first equilibrated with ABleb at a concentration of 1 μM, which does not suppress blebbing even on a long timescale (Figure 4A). Following 2P irradiation, bleb formation of the tattooed cell was abolished, while the surrounding, non-irradiated cells kept blebbing continuously (Figure 4B; Movies S2 and S3). During irradiation in the presence of 1 mMABleb, the fluorescence of the cell increased due to the photoreaction of ABleb (Figure 4C), while tattooing in the presence of 1 mM NBleb did not result in an increase in fluorescence. We followed the blebbing activity of cells indicated by blebbing indices (Charras et al., 2005) after tattooing with ABleb and found a similar effect to that of treatment with a

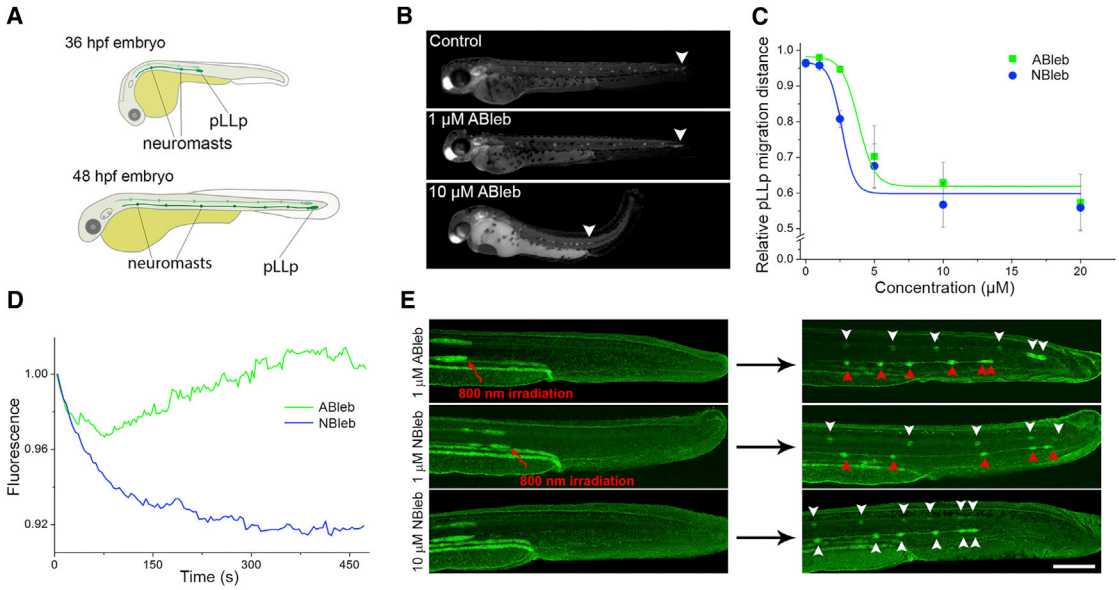

Figure 3. Molecular Tattooing Unveils the Autonomous Function of Non-muscle Myosin 2 in the Migration of pLLp of Live Zebrafish Embryos

(A) Schematic drawings of zebrafish embryos displaying the spatial formation of the lateral line.

(B) Fluorescence images of 48 hpf zebrafish embryos incubated in the absence and presence of ABleb in dark for 24 hr. White arrowheads mark the position of the halted pLLps.

(C) Relative distance of pLLp migration in the presence of ABleb or NBleb (1 = distance from the otic vesicle to the tip of the tail). Dose-response curves were fitted to means ± SD (n = 4).

(D) Relative fluorescence change of pLLps in live *cldn:gfp* zebrafish embryo during 2P irradiation in the presence of ABleb or NBleb.

(E) Projected confocal z-stack images of zebrafish embryos with 2P-irradiated pLLps on one side (indicated by red arrows) in the presence of 1 μM ABleb, 1 μM NBleb, and non-irradiated embryo in the presence of 10 μM NBleb. White (non-irradiated) and red (irradiated) arrowheads mark sites of neuromast deposition. See also Movie S1. Scale bar represents 200 μm.

high concentration (10 μM) of ABleb without irradiation (Figure 4D). Tattooing in the presence of the inactive blebbistatin enantiomer ((+)-blebbistatin) (Straight et al., 2003) substituted by an azido group at the same position as ABleb, named (+)-ABleb, had no effect on the blebbing activities of M2 cells. This photoreactive but non-inhibitory derivative of blebbistatin serves as a control for the selectivity of molecular tattooing in vivo. In addition, low ligand concentrations are also in favor of the target-specific photoreaction induced by 2P irradiation.

In order to demonstrate subcellular tattooing of live cells, we irradiated one half of an M2 cell equilibrated with 1 μM ABleb. In the tattooed hemisphere, the increased fluorescence indicated ABleb-myosin 2 covalent complex formation. We followed the diffusion or the migration of ABleb-myosin 2 complexes for 20 min (Figure 4E). The insignificant shape change of the tattooed, brightly fluorescent area indicated that any diffusion or migration of myosin 2-ABleb complexes was slow. A similarly slow movement of blebbistatin-inhibited non-muscle myosin 2 was found in bovine aortic endothelial cells while active non-muscle myosin 2 spread relatively fast in the cell, which was also confirmed by independent fluorescent recovery after photobleaching (FRAP) experiments (Allingham et al., 2005; Breckenridge et al., 2009). The blebbing index of the tattooed hemisphere dropped by 75%, and, interestingly, the blebbing index decreased slightly (30%) in the non-tattooed hemisphere as well (Figure 4F, left panel, and Movies S4 and S5). The asymmetric blebbing of the hemi-tattooed cell indicates an uneven distribution of the active and inhibited myosin 2 molecules, possibly due to the very different diffusion coefficients of the two molecular populations. One of the limitations of subcellular molecular tattooing may be the possible fast diffusion of inhibited and/or active enzyme populations in other systems. On the other hand, bleb size decreased similarly on both the irradiated and non-irradiated sides of the cell (Figure 4F, right panel). The decrease in bleb size refers to an overall drop in the hydrostatic pressure within the cell, equilibrating on the second timescale (Charras et al., 2005), due to a significant amount of inhibited myosin 2 molecules. This pressure drop causes the decrease of the blebbing index on the non-irradiated side as well. The subcellular ABleb tattoo experiment demonstrates that specific targets can be inhibited in the local regions of the cell, revealing both local and global effects within the mechanism of blebbing.

DISCUSSION

The overall goal of targeted drug delivery is to achieve a sustained, target-specific, and localized effect of bioactive compounds. Based on the exploration of a 2P-induced photo-cross-linking reaction, we have developed an optopharmacological tool, molecular tattooing, which meets these three requirements simultaneously. After characterizing and optimizing the technical parameters of molecular tattooing, we demonstrated the potential of the technique by tattooing ABleb into specific regions of whole live animals and subcellular locations of blebbing M2 cells. Molecular tattooing enables us to understand how spatial

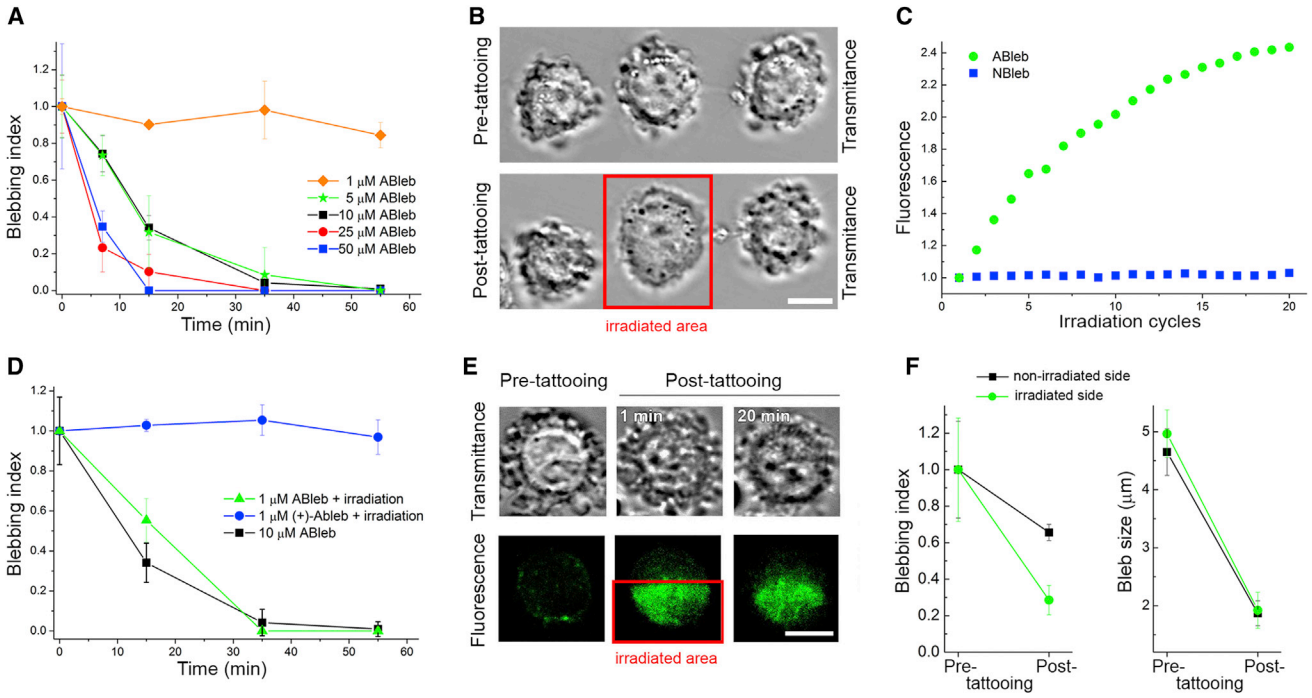

Figure 4. Cellular and Subcellular Targeting of Myosin 2 in Live M2 Cells Reveal Mechanistic Details of Myosin 2 Function in Blebbing

(A) M2 cells were incubated at different concentrations of ABleb for 60 min in the dark and their blebbing indices were determined at the indicated times.

(B) 2PM bright-field images of blebbing M2 cells in the presence of 1 μM ABleb before (pre-tattooing) and after (post-tattooing) 2P irradiating one of them (indicated by red square). See also Movies S2 and S3. Scale bar represents 10 μm.

(C) Relative fluorescence of M2 cells during 2P irradiation cycles in the presence of 1 μM ABleb or NBleb.

(D) Normalized blebbing indices of M2 cells in the presence of 1 μM ABleb or 1 μM (+)-ABleb following 2P irradiation and 10 μM ABleb without irradiation.

(E) Fluorescence (lower panels) and bright-field (upper panels) images of an M2 cell before (pre-tattooing) and after 2P irradiation (post-tattooing) half of the cell (red square) in the presence of 1 μM ABleb. The diffusion of ABleb-myosin 2 covalent complexes was followed for 20 min.

(F) Normalized blebbing indices (left panel) and bleb size (right panel) of irradiated and non-irradiated sides of hemi-tattooed M2 cells pre- and 20 min post-tattooing. Data represent means ± SD (n = 4). See also Movies S4 and S5. Scale bar represents 10 μm.

confinement affects the functions of an enzymatic action revealing experimentally features of biological mechanisms that are currently inaccessible.

A few technical approaches are available for localized targeting (Table 2). An intriguing approach for subcellular targeting is extracellular local perfusion of adherent cells when the bioactive compound is pipetted into a continuous laminar fluid flow, bathing part of the cell with the drug. Subcellular perfusion can also be achieved by microfluidic devices, which create microenvironments by fluidically isolating subcellular compartments of cultured cells. This isolation enables localized treatment with any bioactive compound. With the help of this technique, researchers were able to selectively and locally label targets with fluorescent ligands (O'Connell et al., 2001), track synapse-to-nucleus signaling of neurons (Taylor et al., 2010), or investigate the effect of local manipulation on global cellular processes (e.g. cytokinesis, blebbing) (Charras et al., 2005). Advantages of the method include that any bioactive compound can be applied as no chemical modification is involved; furthermore, temporal control (on the seconds or minutes scale) and reversible treatment are both achievable.

However, due to diffusion and potential compartmentalization processes within the cell, the local concentrations and the intracellular areas affected are indefinite. Other technical approaches for subcellular targeting use photoactivatable ligands and light for the localization and timing of treatment, and form two separate branches of optopharmacology, depending on the type of photoreaction. The type of photoactive moiety attached to the bioactive compound is either a protecting group of caged compounds that can be photolyzed or an azobenzene moiety of photochromic ligands or photoswitches that undergoes a reversible *cis-trans* photoisomerization. Uncaging is undoubtedly advantageous for rapid, extremely precise, subfemtoliter activation of bioactive compounds (Matsuzaki et al., 2008; Mattison et al., 2014; Tonnesen et al., 2014), whereas photoswitch is a promising technique for the rapid, reversible perturbation of biological processes (Mourot et al., 2013). Both techniques involve chemical modification of the ligands, thereby limiting the arsenal of available compounds (Broichhagen et al., 2014). Another drawback of caged molecules and photoswitches is that their systemic administration at the required relatively high ligand concentrations may result in unwanted systemic effects that undermine the specificity of their targeting. In addition, in both methods, the targeted area is transient and indefinite due to rapid diffusion of the active compound.

Molecular tattooing presented in this study overcomes the limitations of local perfusion and almost all the drawbacks of other optopharmacological techniques (Table 2) but retaining the need

Table 2. Technical Approaches for Subcellular Drug Targeting

Targeting Techniques	Subcellular Local Perfusion	Uncaging	Photoswitch	Molecular Tattoo
Effect	local effect	systemic or transiently local	transiently local	permanent local
Administration of the compound	local	systemic	systemic	systemic
	active ligand $>EC_{50}$	caged ligand $\gg EC_{50}$	switchable ligand $>EC_{50}$	photoreactive ligand $\ll EC_{50}$
Modes of targeting	direction of flow	UV, 2P	UV (VIS)	2P
Strength	unmodified ligand reversible	rapid switch-on subfemtoliter targeted area	rapid, reversible switch on/off	subfemtoliter targeted area permanent effect no systemic drug effects
Weakness	low resolution indefinite effect localization in vitro relatively slow temporal control (seconds scale)	low uncaging yield systemic side effects transient effect due to diffusion ligand modification	systemic side effect transient effect due to diffusion phototoxicity ligand modification	relatively slow temporal control (seconds scale) irreversible ligand modification

for chemical modification of the ligands. In molecular tattooing, we can target with subfemtoliter resolution resulting in permanent effect confinement of the bioactive compounds. Temporal control of the effect is determined by the turnover of the target protein, while in the case of subcellular targeting, the localization also depends on diffusion of the covalent ligand-target complex. Systemic effects outside the targeted area and side effects of the compound are negligible because the covalent ligand-target complex is enriched at low concentrations of the photoreactive compound ($\ll EC_{50}$) by sequential 2P laser scanning similar to sequential PAL. This advantage is especially well demonstrated by the highly confined effects of ABleb during molecular tattooing of zebrafish embryos at low compound concentrations compared with the severe systemic effects (curved body shape, cardiac edema, eventually lethality) of the inhibitor at high concentrations (Figure 3B). Molecular tattoos comprise irreversible drug-target complexes and this irreversibility might be a limitation in some applications. Temporal control of the switch-on of the drug effect depends on the size of the targeted area, the speed of laser scanning, and the binding kinetics of the drug. Recent advances in 2P microscopy instrumentation, especially in acousto-optic 3D scanning methods, have enabled rapid, practically simultaneous molecular tattooing of multiple target areas (Fernandez-Alfonso et al., 2014; Go et al., 2013; Katona et al., 2012).

The availability of photoreactive ligands is key for propagation of molecular tattooing in the life sciences. Several azidated bioactive compounds are commercially available and have been synthesized (Table 3) (Sumranjit and Chung, 2013; Vodovozova, 2007). The chemical synthesis of azidated aromatic molecules can be efficiently performed by a halogen azide exchange reaction of aryl-halide precursors. Fortunately, halo derivatives of bioactive compounds are commonly available because in the case of many pharmaceutical agents, the synthetic route of their halo (iodo) derivative has been explored due to the need for radiolabeling for receptor binding assays, absorption, distribution, metabolism, and excretion studies, or single photon emission computed tomography imaging. Importantly, structure-activity relationship (SAR) studies for these halo derivative drugs have also been performed in order to evaluate the effect of substitution on the bioactivity of the compound. Furthermore, in the drug discovery pipeline, SAR studies generate a great number of halo-substituted derivatives of leading compounds providing valuable synthetic routes and SAR data about the modifiable positions; if halo substitution has no significant effect on the binding properties of the compound, it is a very good indication that azido substitution will not either.

Although azido substitution is the smallest possible modification to obtain a photoreactive compound, benzophenone and diazirine derivatives may provide further opportunities for molecular tattooing (Table 3). These compounds have become widely used in PAL, however, their low absorption coefficient may limit their in vivo application in molecular tattooing. The conditions for molecular tattooing must be optimized between the efficiency of the photoreaction and laser phototoxicity. The former has a quadratic dependency on the laser intensity and the compound's absorption coefficient at the 2P irradiation wavelength applied, while phototoxicity has a weaker dependency on laser intensity. Thus, choosing the optimal intensity and wavelength is crucial in the process of optimization. The Ti:Sa laser source applied in 2PM is tunable between 690 and 1,040 nm, which is suitable for photoreactive ligands that have significant absorption above 350 nm. Examples of such molecules from different branches of biological research are the myosin 2 inhibitor, ABleb (Kepiro et al., 2012) (ε_{400} = 4,500 M^{-1} cm^{-1}), the AMPA and kainate receptor antagonist ANQX (Adesnik et al., 2005) (ε_{380} = 8,860 M^{-1} cm^{-1}), the Wnt agonist azidoazakenpaullone (ε_{350} = 19,200 M^{-1} cm^{-1}) or the antipsychotic compound azidoclozapine (ε_{350} = 1,700 M^{-1} cm^{-1}). For ligands possessing absorption at lower wavelengths, recent technology provides wavelength modulation of the Ti:Sa laser by the application of frequency doubling combined with commercially available optical parametric oscillator.

Molecular tattooing provides extremely precise and prolonged target modulation, a feature that opens new research opportunities in several areas of the life sciences. Molecular tattoo can be an advantageous resource in biophysics, enabling researchers to explore different forces and dynamics within the cell by spatiotemporal inhibition of the actomyosin machinery. A molecular tattoo could also be used as a reverse FRAP; a confined group of targeted enzyme molecules is tattooed with a fluorescent inhibitor, then the cellular diffusion coefficient of the inhibitor-enzyme complex may be obtained from the decay in local fluorescence intensity due to the diffusion of the

Table 3. Examples for Bioactive Compounds Suitable for Molecular Tattooing

Azido and Benzophenone Substituted Compounds	Mode of Action
Azidoblebbistatin (Kepiro et al., 2012)	myosin 2 inhibitor
Azidoclozapine	antipsychotic agent
Azidocelecoxib 1 and 2	cyclooxygenase inhibitors
Azidolidocaine	Na-channel blocker
AzidoQX314	Na-channel blocker
Azidocarbamazepine	Na-channel blocker
Azidoriluzole	Na-channel blocker
Perphenazine-azidobenzoate	antipsychotic agent
Azidosulpiride	antipsychotic agent
Azidoazakenpaullone	Wnt agonists
6-Azido-7-nitro-1,4-dihydroquinoxaline-2,3-dione (ANQX) (Cruz et al., 2008)	antagonist of α-amino-3-hydroxy-5-methyl-4-isoxazolepropionic acid (AMPA) receptor
Benzoyl-ATP (Bhargava et al., 2012)	ATPases, P2X receptor agonist modulator
p-Benzoyl-L-phenylalanine (Kauer et al., 1986)	part of small peptides acting as ligand
Benzoylcholine (Nirthanan et al., 2005)	nicotinic acetylcholine receptor agonist
Ethidiumdiazide (Pratt et al., 2000)	nicotinic acetylcholine receptor antagonist
Ro 15-4513 (Duncalfe and Dunn, 1996)	γ-aminobutyric acid A ($GABA_A$) receptor partial inverse agonist
Benzophenone substituted diketo acid derivatives (Zhang et al., 2004)	HIV-1 integrase inhibitor
Azido derivatives of 3-(2-methyl-1*H*-indol-3-yl)-1-(4-pyridinyl)-2-propen-1-one (MIPP) (Robinson et al., 2012)	methuosis inducer
Azido-nitrobenzoyl derivatives of testosterone (Mappus et al., 2000)	androgen receptor agonist
Azidoauxin (Zettl et al., 1994)	glutathione *S*-transferase binding
Haloperidol-azidobenzoate (Kanety and Fuchs, 1988)	antipsychotic agent
Azidofluorescein (Salic and Mitchison, 2008)	fluorophore
Azidocoumarin (Stoianov and Robinson, 2012)	push-and-pull fluorophore

molecules within the living cell. Furthermore, with the advent of in vivo superresolution microscopies (Gao et al., 2012), individual molecules of the optopharmacologically labeled enzymes may be followed. Comparing the results of molecular tattooing with FRAP, activity-mobility relationships of enzymes and mechanistic details of their action can be explored. By tattooing half of an M2 cell with ABleb, we were able to show that the inhibited myosin 2 molecules cannot diffuse freely, which indicates that dispersion of myosin 2 within the cell is an active process. In developmental biology, autonomous and non-autonomous functions of cells or organs can be separated, which was hitherto only possible by transplantation experiments (Li et al., 2011; White et al., 2008). Accordingly, local inhibition of the activity of myosin 2 in the migrating pLLp by molecular tattooing demonstrated that myosin activity in this developmental process is autonomous. Further developmental mechanisms can be unveiled by spatiotemporal inhibition or activation of signaling pathways. By molecular tattooing, scientists will be able to map the subcellular anatomy of signaling networks providing new levels of understanding not only in developmental biology but also in cell biology, immunology, and genetics. As the resolution of a molecular tattoo is subfemtoliter, prolonged modulation of neurons or even single synapses is feasible, enabling new methodological approaches in neurophysiology. Since long-term activation or inhibition of single synapses can be achieved by molecular tattooing, fundamental biological questions may become experimentally accessible, i.e. what is the function of single synapses in multi-synaptic connections or how are the long-term potentiation of neuronal networks and synaptic plasticity related to memory formation, learning, or drug addiction.

SIGNIFICANCE

With the molecular tattooing technique, target-specific drug effects can be confined in vivo into even a subfemtoliter volume without any systemic effects and side effects outside the targeted area. We demonstrated the potential of molecular tattooing as a novel optopharmacological tool with local inhibition of myosin 2 by 2P-irradiation of ABleb into the developing lateral line of live zebrafish and into subcellular regions of blebbing human melanoma cells. We revealed that myosin 2 has an autonomous role in lateral line development of zebrafish and demonstrated local and global effects of local myosin 2 inhibition in the blebbing of melanoma cells. Importantly, a series of photoreactive bioactive ligands are already available for a wide variety of targets and further photoreactive compounds can be synthesized easily from existing drug derivatives. Thereby, local targeting with molecular tattooing will reveal hidden molecular mechanistic details in various research fields by dissecting specific interactions of complex collective processes such

as organ development or activity of a multi-synaptic neuronal network, or by locally modulating processes in cell movement, blebbing, cytokinesis, or signaling.

EXPERIMENTAL PROCEDURES

Reagents

ABleb (Kepiro et al., 2012), NBleb (Képiró et al., 2014), (+)-ABleb, and AFluo (Salic and Mitchison, 2008) were synthesized in our laboratory according to published protocols. Stock solutions of the inhibitors were dissolved in DMSO (Sigma-Aldrich), protected from light, and stored at −20°C.

Fluorescence Spectroscopic Measurements

A 5-μM ABleb solution was prepared in 0.8 M Tris-HCl (pH 9). The high concentration of Tris-HCl ensured that photoactivated ABleb attached mainly to primary amine (nucleophile). Fluorescence emission spectra (λ_{ex} = 400) were recorded prior to and following irradiation of ABleb at λ_{irrad} = 400 ± 18 nm for 10 min using an Edinburgh Instruments F900 Fluorescence Spectrometer equipped with a 450-W xenon lamp. The intensity of excitation during the emission spectral scan was low enough that no significant photoreaction of ABleb occurred. The applied λ_{ex} and λ_{irrad} correspond to half of the wavelength used in 2PM.

Two-Photon Microscope

2PM of the samples was carried out in a Femtonics 2P microscope equipped with a mode-locked MaiTai Deep See Laser source (Spectra-Physics) with 100-fs pulse width and 80-MHz repetition rate. Image acquisition was performed using MES software (Femtonics).

Photoactivation of ABleb and AFluo in the Function of 2P Laser Power

10 mM ABleb or AFluo in DMSO was loaded into glass capillaries (0.2 μm inner diameter) and the sample was raster scanned (xy scanned) (λ_{ex} = 800 nm) for 2 min with the 2PM at different laser powers using a 10×/0.4 objective (Olympus UPLSAPO). During the scan, the step size and the dwell time were 3 μm and 2.72 μs, respectively. Following irradiation, the content of the capillary was transferred into high-performance liquid chromatography buffer (water/acetonitrile 1:1, supplemented with 0.1% trifluoroacetic acid), and the sample was subjected to LC-MS analysis using a C18 column and isocratic elution (water/acetonitrile 1:1, 0.1% trifluoroacetic acid). The resulted data points presented in Figure 1A were fitted with $y = y_0 + Aexp(-(kI)^2/2)$ where y is the conversion of the photoreaction, A is the amplitude, k is the rate constant, and I is the power of the laser.

Measuring the Lateral (xy) and z Dimensions of V_{2PR}

Assay buffer (40 mM NaCl, 4 mM $MgCl_2$, 20 mM HEPES [pH 7.3]) was supplemented with 0.16 g ml^{-1} type B gelatin (Sigma-Aldrich) and the mixture was heated for 20 min at 40°C. ABleb in DMSO was added to the warm gelatin at a final concentration of 50 μM and the mixture was pipetted into an imaging dish (MoBiTec, Imaging dish 1.5). After cooling, 300 μl of 50 μM ABleb in assay buffer was pipetted on to the gel surface to circumvent drying. Three letters "M" were engraved (by line scanning, i.e. one-dimensional scanning) in the gel with 2PM irradiation (λ_{ex} = 800 nm), each using different objective lenses: 10×/0.4 NA UPLSAPO (Olympus), 40×/0.8 NA LUMPLFLN W (Olympus), and 60×/1.35 NA UPLSAPO O (Olympus). The irradiation settings were as follows: dwell time = 21.76 μs, step size = 0.05 μm, scanning time = 50 s. Laser power was 20%, 25% and 40% for the 10×, 40×, and 60× objectives, respectively (100% laser power = 904 mW). The line-scanned areas were imaged by z sectioning (2-, 1-, and 1-μm z-steps with the 10×, 40×, and 60× objectives, respectively). Image analysis was performed using ImageJ software (public domain).

In Vitro Covalent Crosslinking of the Myosin Motor Domain and ABleb

34 μM isolated myosin *Dictyostelium* motor domain (Kepiro et al., 2012) was treated with 50 μM ABleb. 1 μl of the sample was UV irradiated with a transilluminator table (Benchtop 3UV Transilluminator, 8 W) for 30 s at 0°C. 1 μl of the samples was 2P irradiated at 800 nm with a focused or unfocused laser beam using a 10×/0.4 objective, 80% laser power with 3-μm step size, and 2.72-μs dwell time for 15 min at 0°C. The crosslinked samples were analyzed by LC-MS.

Fish Husbandry and Treatment of Embryos

Transgenic *Tg(−8.0cldnb:lynEGFP)zf106* (*cldn:gfp*) fish stocks (Haas and Gilmour, 2006) were maintained in the animal facility of Eötvös Loránd University according to standard protocols (Westerfield, 2000). For tattooing experiments, embryos 1 day post fertilization were dechorionated and incubated in the dark for 10 min in standard E3 embryo medium containing ABleb, NBleb, or DMSO as a control. Subsequently, they were transferred to preheated (40°C) 1% low-melting-point agarose (Sigma-Aldrich) and placed in imaging dishes (MoBiTec, Imaging dish 1.5). After cooling, the embedded embryos were incubated in E3 medium containing DMSO or the inhibitors for 10 min. The concentration of DMSO in the E3 buffer was 0.1% throughout the experiments. In the case of systemic treatment (with 10 μM NBleb), the embryos were imaged with confocal microscopy (z stack every 10 min for 12 hr, λ_{ex} = 488 nm, Plan-Apochromat 10×/0.45 NA M27, Zeiss Zen driver, and image analysis software).

2P Irradiation of Zebrafish Embryos

2P irradiation of molecular tattooing was performed by raster scanning of the pLLp at λ_{ex} = 800 nm for 8 min using a 10×/0.4 NA UPLSAPO objective (Olympus). The parameters for the raster scan were as follows: dwell time = 21.76 μs, step size = 0.1 μm, laser power = 3%. The duration of one scan was 3 s. Following irradiation, the embryos were imaged with confocal microscopy as described above. Movies of the migrating pLLp are at 10 frames per second (fps). All protocols used in this study were approved by the Hungarian National Food Chain Safety Office (permit number XIV-I-001/515-4/2012).

Maintenance of M2 Cell Culture

M2 human melanoma cells (Salic and Mitchison, 2008) were grown in MEM (Lonza) supplemented with 8% newborn calf serum (Sigma) and 2% fetal calf serum. The cell culture was maintained in a humidified atmosphere of 5% CO_2 at 37°C. Cells were grown as monolayers in T 75-cm^2 culture flasks and subcultured by the addition of 0.02% EDTA (200 mg l^{-1}) 2–3 times per week upon reaching 90% confluence.

2P Irradiation of M2 Cells

Experiments were performed 18 hr after plating onto imaging dishes (MoBiTec, Imaging dish 1.0), when nearly 90% of the cells displayed extensive blebbing (Cunningham, 1995). Prior to 2P irradiation, cells were incubated for 20 min in PBS (140 mM NaCl, 2.7 mM KCl, 10.1 mM Na_2HPO_4, 1.8 mM KH_2PO_4 [pH 7.9]) containing 1 μM ABleb or (+)-ABleb. The concentration of DMSO in PBS was 0.1% throughout the experiments. Tattooing experiments were performed using a 60×/1.35 NA UPLSAPO O objective (Olympus) at λ_{ex} = 900 nm. The parameters of z-sectioning were the following: dwell time = 43.52 μs, step size = 0.1 μm, laser power = 2.5%, z step = 2 μm, number of slices = 8. Images were analyzed with ImageJ software. Blebbing indices are defined as the number of blebs observed during a given period of time within a given perimeter of the cell (Charras et al., 2005).

SUPPLEMENTAL INFORMATION

Supplemental Information includes five movies and can be found with this article online at http://dx.doi.org/10.1016/j.chembiol.2015.03.013.

AUTHOR CONTRIBUTIONS

M.K. performed in vitro and in vivo experiments, B.H.V. performed in vivo and cellular experiments, contributing equally to this study. M.K., B.H.V., M.S.Z.K., M.V., and A.M.C. designed the research. M.K., B.H.V., and A.M.C. analyzed the data. M.K., B.H.V., A.A.R., M.S.Z.K., M.V., and A.M.C. wrote the manuscript.

ACKNOWLEDGMENTS

M2 cells were a kind gift from Tom Stossel and Fumihiko Nakamura (Brigham & Women's Hospital, Harvard Medical School, Translational Medicine Division).

A.M.C. is funded by the European Research Council (European Community's Seventh Framework Program (FP7/2007-2013)/ERC grant agreement no. 208319), ERC-PoC (grant agreement no. 620315) and Hungarian Research and Innovation Fund (KTIA_AIK_12-1-2013-0005). M.V. is a János Bolyai Fellow of the Hungarian Academy of Sciences.

Received: January 15, 2015
Revised: March 11, 2015
Accepted: March 13, 2015
Published: April 16, 2015

REFERENCES

Adesnik, H., Nicoll, R.A., and England, P.M. (2005). Photoinactivation of native AMPA receptors reveals their real-time trafficking. Neuron *48*, 977–985.

Allingham, J.S., Smith, R., and Rayment, I. (2005). The structural basis of blebbistatin inhibition and specificity for myosin II. Nat. Struct. Mol. Biol. *12*, 378–379.

Artamonov, M.V., Momotani, K., Stevenson, A., Trentham, D.R., Derewenda, U., Derewenda, Z.S., Read, P.W., Gutkind, J.S., and Somlyo, A.V. (2013). Agonist-induced Ca2+ sensitization in smooth muscle: redundancy of Rho guanine nucleotide exchange factors (RhoGEFs) and response kinetics, a caged compound study. J. Biol. Chem. *288*, 34030–34040.

Augustine, G.J. (1994). Combining patch-clamp and optical methods in brain slices. J. Neurosci. Methods *54*, 163–169.

Bhargava, Y., Rettinger, J., and Mourot, A. (2012). Allosteric nature of P2X receptor activation probed by photoaffinity labelling. Br. J. Pharmacol. *167*, 1301–1310.

Breckenridge, M.T., Dulyaninova, N.G., and Egelhoff, T.T. (2009). Multiple regulatory steps control mammalian nonmuscle myosin II assembly in live cells. Mol. Biol. Cell *20*, 338–347.

Broichhagen, J., Jurastow, I., Iwan, K., Kummer, W., and Trauner, D. (2014). Optical control of acetylcholinesterase with a tacrine switch. Angew. Chem. Int. Ed. Engl. *53*, 7657–7660.

Charras, G., and Paluch, E. (2008). Blebs lead the way: how to migrate without lamellipodia. Nat. Rev. Mol. Cell Biol. *9*, 730–736.

Charras, G.T., Yarrow, J.C., Horton, M.A., Mahadevan, L., and Mitchison, T.J. (2005). Non-equilibration of hydrostatic pressure in blebbing cells. Nature *435*, 365–369.

Cheung, A., Dantzig, J.A., Hollingworth, S., Baylor, S.M., Goldman, Y.E., Mitchison, T.J., and Straight, A.F. (2002). A small-molecule inhibitor of skeletal muscle myosin II. Nat. Cell Biol. *4*, 83–88.

Cruz, L.A., Estebanez-Perpina, E., Pfaff, S., Borngraeber, S., Bao, N., Blethrow, J., Fletterick, R.J., and England, P.M. (2008). 6-Azido-7-nitro-1,4-dihydroquinoxaline-2,3-dione (ANQX) forms an irreversible bond to the active site of the GluR2 AMPA receptor. J. Med. Chem. *51*, 5856–5860.

Cunningham, C.C. (1995). Actin polymerization and intracellular solvent flow in cell surface blebbing. J. Cell Biol. *129*, 1589–1599.

Denk, W., Strickler, J.H., and Webb, W.W. (1990). Two-photon laser scanning fluorescence microscopy. Science *248*, 73–76.

Denk, W., Delaney, K.R., Gelperin, A., Kleinfeld, D., Strowbridge, B.W., Tank, D.W., and Yuste, R. (1994). Anatomical and functional imaging of neurons using 2-photon laser scanning microscopy. J. Neurosci. Methods *54*, 151–162.

Duncalfe, L.L., and Dunn, S.M. (1996). Mapping of GABAA receptor sites that are photoaffinity-labelled by [3H]flunitrazepam and [3H]Ro 15-4513. Eur. J. Pharmacol. *298*, 313–319.

Ernst, S., Liu, K., Agarwala, S., Moratscheck, N., Avci, M.E., Dalle Nogare, D., Chitnis, A.B., Ronneberger, O., and Lecaudey, V. (2012). Shroom3 is required downstream of FGF signalling to mediate proneuromast assembly in zebrafish. Development *139*, 4571–4581.

Fackler, O.T., and Grosse, R. (2008). Cell motility through plasma membrane blebbing. J. Cell Biol. *181*, 879–884.

Fernandez-Alfonso, T., Nadella, K.M., Iacaruso, M.F., Pichler, B., Ros, H., Kirkby, P.A., and Silver, R.A. (2014). Monitoring synaptic and neuronal activity in 3D with synthetic and genetic indicators using a compact acousto-optic lens two-photon microscope. J. Neurosci. Methods *222*, 69–81.

Fleet, G.W.J., Porter, R.R., and Knowles, J.R. (1969). Affinity labelling of antibodies with aryl nitrene as reactive group. Nature *224*, 511–512.

Friedl, P., and Gilmour, D. (2009). Collective cell migration in morphogenesis, regeneration and cancer. Nat. Rev. Mol. Cell Biol. *10*, 445–457.

Gao, L., Shao, L., Higgins, C.D., Poulton, J.S., Peifer, M., Davidson, M.W., Wu, X., Goldstein, B., and Betzig, E. (2012). Noninvasive imaging beyond the diffraction limit of 3D dynamics in thickly fluorescent specimens. Cell *151*, 1370–1385.

Geurink, P.P., Prely, L.M., van der Marel, G.A., Bischoff, R., and Overkleeft, H.S. (2012). Photoaffinity labeling in activity-based protein profiling. Top. Curr. Chem. *324*, 85–113.

Go, M.A., To, M.S., Stricker, C., Redman, S., Bachor, H.A., Stuart, G.J., and Daria, V.R. (2013). Four-dimensional multi-site photolysis of caged neurotransmitters. Front. Cell. Neurosci. *7*, 231.

Guo, Y.M., Chen, S., Shetty, P., Zheng, G., Lin, R., and Li, W.H. (2008). Imaging dynamic cell-cell junctional coupling in vivo using Trojan-LAMP. Nat. Methods *5*, 835–841.

Haas, P., and Gilmour, D. (2006). Chemokine signaling mediates self-organizing tissue migration in the zebrafish lateral line. Dev. Cell *10*, 673–680.

Kanety, H., and Fuchs, S. (1988). Immuno-photoaffinity labeling of the D2-dopamine receptor. Biochem. Biophys. Res. Commun. *155*, 930–936.

Kaplan, J.H., and Somlyo, A.P. (1989). Flash photolysis of caged compounds: new tools for cellular physiology. Trends Neurosci. *12*, 54–59.

Katona, G., Szalay, G., Maak, P., Kaszas, A., Veress, M., Hillier, D., Chiovini, B., Vizi, E.S., Roska, B., and Rozsa, B. (2012). Fast two-photon in vivo imaging with three-dimensional random-access scanning in large tissue volumes. Nat. Methods *9*, 201–208.

Kauer, J.C., Erickson-Viitanen, S., Wolfe, H.R., Jr., and DeGrado, W.F. (1986). p-Benzoyl-L-phenylalanine, a new photoreactive amino acid. Photolabeling of calmodulin with a synthetic calmodulin-binding peptide. J. Biol. Chem. *261*, 10695–10700.

Képiró, M.V., Várkuti, B.H., Végner, L., Vörös, G., Hegyi, G., Varga, M., and Málnási-Csizmadia, A. (2014). Para-nitroblebbistatin, the non-cytotoxic and photostable myosin II inhibitor. Angew. Chem. Int. Ed. Engl. *53*, 8211–8215.

Képiró, M., Várkuti, B.H., Bodor, A., Hegyi, G., Drahos, L., Kovács, M., and Málnási-Csizmadia, A. (2012). Azidoblebbistatin, a photoreactive myosin inhibitor. Proc. Natl. Acad. Sci. USA *109*, 9402–9407.

Kolega, J. (2004). Phototoxicity and photoinactivation of blebbistatin in UV and visible light. Biochem. Biophys. Res. Commun. *320*, 1020–1025.

Kramer, R.H., Mourot, A., and Adesnik, H. (2013). Optogenetic pharmacology for control of native neuronal signaling proteins. Nat. Neurosci. *16*, 816–823.

Li, P., White, R.M., and Zon, L.I. (2011). Transplantation in zebrafish. Methods Cell Biol. *105*, 403–417.

Li, Z., Stankevicius, E., Ajami, A., Raciukaitis, G., Husinsky, W., Ovsianikov, A., Stampfl, J., and Liska, R. (2013). 3D alkyne-azide cycloaddition: spatiotemporally controlled by combination of aryl azide photochemistry and two-photon grafting. Chem. Commun. *49*, 7635–7637.

Ma, E.Y., and Raible, D.W. (2009). Signaling pathways regulating zebrafish lateral line development. Curr. Biol. *19*, R381–R386.

Maier, W., Corrie, J.E., Papageorgiou, G., Laube, B., and Grewer, C. (2005). Comparative analysis of inhibitory effects of caged ligands for the NMDA receptor. J. Neurosci. Methods *142*, 1–9.

Mappus, E., Chambon, C., Fenet, B., Rolland de Ravel, M., Grenot, C., and Cuilleron, C.Y. (2000). Synthesis of (5-azido-2-nitrobenzoyl)amido, (4-azido-2-nitrophenyl)amino, and (5-azido-2-nitro-3,4, 6-trifluorophenyl)amino derivatives of 17alpha-methylamino-, 17alpha-ethylamino-, and 17alpha-propylamino-5alpha-dihydrotestosterone as reagents of different linker lengths for the photoaffinity labeling of sex hormone binding globulins and androgen receptors. Steroids *65*, 459–481.

Matsuzaki, M., Ellis-Davies, G.C., and Kasai, H. (2008). Three-dimensional mapping of unitary synaptic connections by two-photon macro photolysis of caged glutamate. J. Neurophysiol. *99*, 1535–1544.

Matsuzaki, M., Hayama, T., Kasai, H., and Ellis-Davies, G.C. (2010). Two-photon uncaging of gamma-aminobutyric acid in intact brain tissue. Nat. Chem. Biol. *6*, 255–257.

Mattison, H.A., Bagal, A.A., Mohammadi, M., Pulimood, N.S., Reich, C.G., Alger, B.E., Kao, J.P., and Thompson, S.M. (2014). Evidence of calcium-permeable AMPA receptors in dendritic spines of CA1 pyramidal neurons. J. Neurophysiol. *112*, 263–275.

Mayer, G., and Heckel, A. (2006). Biologically active molecules with a "light switch". Angew. Chem. Int. Ed. Engl. *45*, 4900–4921.

McCray, J.A., and Trentham, D.R. (1989). Properties and uses of photoreactive caged compounds. Annu. Rev. Biophys. Biophys. Chem. *18*, 239–270.

McCray, J.A., Herbette, L., Kihara, T., and Trentham, D.R. (1980). A new approach to time-resolved studies of ATP-requiring biological systems; laser flash photolysis of caged ATP. Proc. Natl. Acad. Sci. USA *77*, 7237–7241.

Mourot, A., Tochitsky, I., and Kramer, R.H. (2013). Light at the end of the channel: optical manipulation of intrinsic neuronal excitability with chemical photoswitches. Front. Mol. Neurosci. *6*, 5.

Nguyen, Q.N., Chavli, R.V., Marques, J.T., Conrad, P.G., Jr., Wang, D., He, W., Belisle, B.E., Zhang, A., Pastor, L.M., Witney, F.R., et al. (2006). Light controllable siRNAs regulate gene suppression and phenotypes in cells. Biochim. Biophys. Acta *1758*, 394–403.

Nirthanan, S., Ziebell, M.R., Chiara, D.C., Hong, F., and Cohen, J.B. (2005). Photolabeling the Torpedo nicotinic acetylcholine receptor with 4-azido-2,3,5,6-tetrafluorobenzoylcholine, a partial agonist. Biochemistry *44*, 13447–13456.

O'Connell, C.B., Warner, A.K., and Wang, Y. (2001). Distinct roles of the equatorial and polar cortices in the cleavage of adherent cells. Curr. Biol. *11*, 702–707.

Parker, I., and Ivorra, I. (1993). Confocal microfluorimetry of Ca2+ signals evoked in *Xenopus* oocytes by photoreleased inositol trisphosphate. J. Physiol. *461*, 133–165.

Pratt, M.B., Pedersen, S.E., and Cohen, J.B. (2000). Identification of the sites of incorporation of [3H]ethidium diazide within the Torpedo nicotinic acetylcholine receptor ion channel. Biochemistry *39*, 11452–11462.

Robinson, M.W., Overmeyer, J.H., Young, A.M., Erhardt, P.W., and Maltese, W.A. (2012). Synthesis and evaluation of indole-based chalcones as inducers of methuosis, a novel type of nonapoptotic cell death. J. Med. Chem. *55*, 1940–1956.

Salic, A., and Mitchison, T.J. (2008). A chemical method for fast and sensitive detection of DNA synthesis in vivo. Proc. Natl. Acad. Sci. USA *105*, 2415–2420.

Singh, A., Thornton, E.R., and Westheimer, F.H. (1962). The photolysis of diazoacetylchymotrypsin. J. Biol. Chem. *237*, 3006–3008.

Stoianov, S.V., and Robinson, H.D. (2012). Two-photon activated two-photon fluorescence and binding of azidocoumarin in a gelatin matrix. J. Fluoresc. *22*, 1291–1300.

Straight, A.F., Cheung, A., Limouze, J., Chen, I., Westwood, N.J., Sellers, J.R., and Mitchison, T.J. (2003). Dissecting temporal and spatial control of cytokinesis with a myosin II Inhibitor. Science *299*, 1743–1747.

Sumranjit, J., and Chung, S.J. (2013). Recent advances in target characterization and identification by photoaffinity probes. Molecules *18*, 10425–10451.

Taylor, A.M., Dieterich, D.C., Ito, H.T., Kim, S.A., and Schuman, E.M. (2010). Microfluidic local perfusion chambers for the visualization and manipulation of synapses. Neuron *66*, 57–68.

Tonnesen, J., Katona, G., Rozsa, B., and Nagerl, U.V. (2014). Spine neck plasticity regulates compartmentalization of synapses. Nat. Neurosci. *17*, 678–685.

Vodovozova, E.L. (2007). Photoaffinity labeling and its application in structural biology. Biochemistry (Mosc) *72*, 1–20.

Westerfield, M. (2000). The Zebrafish Book. A Guide for the Laboratory Use of Zebrafish (*Danio rerio*), Fourth Edition. (University of Oregon Press).

White, R.M., Sessa, A., Burke, C., Bowman, T., LeBlanc, J., Ceol, C., Bourque, C., Dovey, M., Goessling, W., Burns, C.E., et al. (2008). Transparent adult zebrafish as a tool for in vivo transplantation analysis. Cell Stem Cell *2*, 183–189.

Williams, R.M., Piston, D.W., and Webb, W.W. (1994). Two-photon molecular excitation provides intrinsic 3-dimensional resolution for laser-based microscopy and microphotochemistry. FASEB J. *8*, 804–813.

Zettl, R., Schell, J., and Palme, K. (1994). Photoaffinity labeling of *Arabidopsis thaliana* plasma membrane vesicles by 5-azido-[7-3H]indole-3-acetic acid: identification of a glutathione S-transferase. Proc. Natl. Acad. Sci. USA *91*, 689–693.

Zhang, X., Marchand, C., Pommier, Y., and Burke, T.R., Jr. (2004). Design and synthesis of photoactivatable aryl diketo acid-containing HIV-1 integrase inhibitors as potential affinity probes. Bioorg. Med. Chem. Lett. *14*, 1205–1207.

Zipfel, W.R., Williams, R.M., and Webb, W.W. (2003). Nonlinear magic: multiphoton microscopy in the biosciences. Nat. Biotechnol. *21*, 1369–1377.

